View metadata, citation and similar papers at core.ac.uk

brought to you by CORE

provided by Elsevier - Publisher Connector

Biochimica et Biophysica Acta 1841 (2014) 906–917

Contents lists available at ScienceDirect

Biochimica et Biophysica Acta

journal homepage: www.elsevier.com/locate/bbalip

Endothelial dysfunction in adipose triglyceride lipase deficiency

Astrid Schrammel [a,*], Marion Mussbacher [a], Gerald Wölkart [a], Heike Stessel [a], Karoline Pail [a], Sarah Winkler [a], Martina Schweiger [b], Guenter Haemmerle [b], Wael Al Zoughbi [c], Gerald Höfler [c], Alois Lametschwandtner [d], Rudolf Zechner [b], Bernd Mayer [a]

[a] Department of Pharmacology and Toxicology, University of Graz, Universitätsplatz 2, 8010 Graz, Austria
[b] Department of Molecular Biosciences, University of Graz, Heinrichstrasse 31, 8010 Graz, Austria
[c] Institute of Pathology, Medical University of Graz, Auenbruggerplatz 25, 8010 Graz, Austria
[d] Department of Cell Biology and Physiology, Vessel and Muscle Research Unit, University of Salzburg, Hellbrunnerstrasse 34, 5020 Salzburg, Austria

ARTICLE INFO

Article history:
Received 17 September 2013
Received in revised form 27 February 2014
Accepted 13 March 2014
Available online 21 March 2014

Keywords:
Adipose triglyceride lipase
Endothelial dysfunction
Perivascular inflammation
Endothelial NO synthase
Vascular proteasome

ABSTRACT

Systemic knockout of adipose triglyceride lipase (ATGL), the pivotal enzyme of triglyceride lipolysis, results in a murine phenotype that is characterized by progredient cardiac steatosis and severe heart failure. Since cardiac and vascular dysfunction have been closely related in numerous studies we investigated endothelium-dependent and -independent vessel function of ATGL knockout mice. Aortic relaxation studies and Langendorff perfusion experiments of isolated hearts showed that ATGL knockout mice suffer from pronounced micro- and macrovascular endothelial dysfunction. Experiments with agonists directly targeting vascular smooth muscle cells revealed the functional integrity of the smooth muscle cell layer. Loss of vascular reactivity was restored ~50% upon treatment of ATGL knockout mice with the PPARα agonist Wy14,643, indicating that this phenomenon is partly a consequence of impaired cardiac contractility. Biochemical analysis revealed that aortic endothelial NO synthase expression and activity were significantly reduced in ATGL deficiency. Enzyme activity was fully restored in ATGL mice treated with the PPARα agonist. Biochemical analysis of perivascular adipose tissue demonstrated that ATGL knockout mice suffer from perivascular inflammatory oxidative stress which occurs independent of cardiac dysfunction and might contribute to vascular defects. Our results reveal a hitherto unrecognized link between disturbed lipid metabolism, obesity and cardiovascular disease.

© 2014 The Authors. Published by Elsevier B.V. This is an open access article under the CC BY-NC-ND license (http://creativecommons.org/licenses/by-nc-nd/3.0/).

1. Introduction

Adipose triglyceride lipase (ATGL) has been identified as key enzyme of mammalian lipolysis, *i.e.* the hydrolytic cleavage of triglycerides into free fatty acids and diacylglycerols. ATGL is predominantly expressed in adipose tissue but found to a lesser extent in a variety of other tissues and organs, including kidney, skeletal muscle, and heart. Studies with ATGL knockout (AKO) mice [1] revealed the systemic importance of this lipase. Deletion of the gene encoding for ATGL resulted in a phenotype with massive neutral lipid accumulation in multiple tissues and cell types. ATGL-deficient mice suffer from an overall defect in energy homeostasis, defective thermogenesis, and severe cardiomyopathy, the latter leading to premature death of the animals [1].

In the myocardium ATGL deficiency has been shown to cause age-dependent increase of myocyte lipid droplets in number and size and, in parallel, progressive development of ventricular hypertrophy [1]. Langendorff perfusion experiments of isolated hearts extended these findings, showing that contractile and microvascular responses to ß-adrenergic stimulation by norepinephrine are drastically impaired in ATGL-deficient hearts [2]. Chronic treatment of AKO mice with the peroxisome proliferator receptor α (PPARα) agonist Wy14,643

Abbreviations: ACh, acetylcholine; ATGL, adipose triglyceride lipase; AKO, adipose triglyceride lipase knockout; BIP, binding immunoglobulin protein; BK, bradykinin; BSA, bovine serum albumin; CD31, cluster of differentiation 31; CL, chemiluminescence; CPP, coronary perfusion pressure; DEA/NO, 2,2-diethyl-1-nitroso-oxyhydrazine; DMEM, Dulbecco's Modified Eagle Medium; EDTA, ethylenediaminetetraacetic acid; eNOS, endothelial nitric oxide synthase; GAPDH, glyceraldehyde-3-phosphate dehydrogenase; H&E, hematoxylin and eosin; Hsp90, heat shock protein 90; IL-6, interleukin 6; IRE-1α, inositol-requiring enzyme 1α; Mac-2, galectin-3; MCP-1, monocyte chemotactic protein-1; NLSDM, neutral lipid storage disease with myopathy; NOX, NADPH oxidase; HO-1, heme oxygenase-1; PBS, phosphate-buffered saline; PDI, protein disulfide isomerase; PEG, polyethyleneglycol; PPARα, peroxisome proliferator receptor α; PVAT, perivascular adipose tissue; α-SMA, α-smooth muscle actin; SOD, superoxide dismutase; TG, triacylglycerol; TNFα, tumor necrosis factor α; U 46619, 9,11-dideoxy-9α,11α-epoxymethanoprostaglandin F2α; VASP, vasodilator-stimulated phosphoprotein; pVASP, phosphorylated vasodilator-stimulated phosphoprotein; WAT, white adipose tissue; WT, wild-type; XBP1, X-box-binding protein 1

* Corresponding author. Tel.: +43 316 380 5559; fax: +43 316 380 9890.
E-mail addresses: astrid.schrammel-gorren@uni-graz.at (A. Schrammel), marion.mussbacher@uni-graz.at (M. Mussbacher), gerald.woelkart@uni-graz.at (G. Wölkart), heike.stessel@uni-graz.at (H. Stessel), karoline.pail@uni-graz.at (K. Pail), sarah.winkler@uni-graz.at (S. Winkler), tina.schweiger@uni-graz.at (M. Schweiger), guenter.haemmerle@uni-graz.at (G. Haemmerle), wael.alzoughbi@stud.medunigraz.at (W. Al Zoughbi), gerald.hoefler@medunigraz.at (G. Höfler), Alois.Lametschwandtner@sbg.ac.at (A. Lametschwandtner), rudolf.zechner@uni-graz.at (R. Zechner), mayer@uni-graz.at (B. Mayer).

http://dx.doi.org/10.1016/j.bbalip.2014.03.005
1388-1981/© 2014 The Authors. Published by Elsevier B.V. This is an open access article under the CC BY-NC-ND license (http://creativecommons.org/licenses/by-nc-nd/3.0/).

restored cardiac contractility [2] and several PPARα target genes were markedly downregulated in ATGL-deficient hearts [3], suggesting that impaired PPARα signaling essentially contributes to the observed cardiac phenotype.

A close relationship between chronic heart failure and endothelial dysfunction has been established in laboratory animals and humans (for review, see [4]), and the severity of endothelial dysfunction has been proposed as prognostic factor for the long-term outcome of patients suffering from heart failure [5,6]. It is assumed that impaired left-ventricular function in heart failure significantly reduces shear stress-induced formation of endothelium-derived NO and consequent NO-dependent dilation of vascular smooth muscle cells. Conversely, impaired peripheral vasodilation leads to higher systemic vascular resistance and consequent increased cardiac workload, which aggravates cardiac dysfunction. In addition, reduced myocardial perfusion due to compromised vasodilator capacity of coronary arteries partially contributes to ventricular dysfunction.

Recently, Hirano and colleagues reported about a male patient homozygous for a point mutation in the ATGL gene suffering from severe congestive heart failure and undergoing cardiac transplantation [7]. Biopsies of the explanted heart showed triglycerides accumulating in atherosclerotic lesions of coronary arteries. In addition, cytoplasmatic lipid storage was observed within endothelial cells and foam cells of the intima as well as within smooth muscle cells of the media. In view of this human correlate and concerning the severe cardiac impairments in murine ATGL deficiency we aimed to study micro- and macrovascular function in this animal model.

2. Theory

AKO mice which represent a rodent model of human neutral lipid storage disease with myopathy (NLSDM) [8] suffer from severe cardiac dysfunction due to ectopic triglyceride accumulation in the heart finally leading to premature death of the animals [1]. This study has been designed (i) to investigate vessel function of this animal model with respect to its cardiac phenotype and (ii) to test for a potential role of perivascular adipose tissue (PVAT) in maintenance of vascular tone.

3. Materials and methods

3.1. Mice and experimental groups

Homozygous AKO mice on a C57BL/6 background [1] and age-matched WT littermates were used for this study. After weaning, animals received standard laboratory mouse chow and water *ad libitum*. Animals subjected to the PPARα agonist treatment protocol were fed control diet mixed with 0.1% Wy14,643 (Cayman Chemical, Ann Arbor, MI, USA) for 3 weeks starting at ~7 weeks of age, as previously described [3]. Mice were housed in approved cages and kept on a regular 12 h dark/light cycle. Animals were sacrificed at ~10 weeks of age. All animals received care in accordance with the Austrian law on experimentation with laboratory animals (last amendment, 2012), which is based on the US National Institutes of Health guidelines. The protocol was approved by the Austrian Federal Ministry for Science and Research (BMWF-66.007/0001-ll/3b/2014).

3.2. Isometric tension vasomotor studies

In a first series of vasomotor studies, the response of aortic vessels to endothelium-dependent and -independent relaxing agents was tested in the absence of perivascular adipose tissue (PVAT). Therefore, descending aortas were removed, carefully cleaned from surrounding PVAT and cut into rings of ~3 mm width and mounted in 5 ml-organ baths filled with oxygenated Krebs–Henseleit solution (118.4 mM NaCl, 25 mM $NaHCO_3$, 4.7 mM KCl, 1.2 mM KH_2PO_4, 2.5 mM $CaCl_2$, 1.2 mM $MgCl_2$, 10.1 mM D-glucose; pH 7.4). Care was taken to retain the endothelium for relaxation experiments. Tissues were equilibrated for 60 min by repeatedly adjusting tension to 0.5 g and changing the bath solution. Then, maximal contractile activity was determined with a depolarizing solution of 100 mM K^+. Rings that did not elicit adequate and stable contraction to high K^+ were considered to be damaged and omitted from the study. After washout, tissues were precontracted with the thromboxane mimetic 9,11-dideoxy-9α,11α-epoxy-methanoprostaglandin F2α (U 46619) to an equivalent level of ~1.2 g total tone (*i.e.* ~90% contracture obtained with high K^+). After reaching a stable contraction, cumulative concentration–response curves were established with acetylcholine (ACh; 1 nM–10 μM) or 2,2-diethyl-1-nitroso-oxyhydrazine (DEA/NO; 1 nM–10 μM; Enzo Life Sciences AG, Lausen, Switzerland). The contractile force corresponding to each agonist concentration was recorded and expressed as percent of precontraction (=baseline). To test for the role of NADPH oxidase-derived superoxide, aortic rings were incubated for 30 min in the presence of either gp91ds-*dat* [9] (50 μM; piChem, Graz, Austria) or a combination of cell-permeable superoxide dismutase (PEG-SOD; 100 U/ml) and catalase (PEG-cat; 500 U/ml) prior to addition of ACh or DEA/NO. In a second series of experiments, the role of PVAT was investigated in paired aortic rings prepared either with or without PVAT. Removal of PVAT from one half of the aorta was randomly assigned to avoid any systematic effects due to the repeated use of similar aortic segments. The equilibration period was followed by repeated challenge with 100 mM K^+ solution until the contractile response became reproducible. After determination of the contractile response to increasing isotonic K^+ solutions (15, 30, 60, 100 mM), cumulative concentration–response curves to U46619 (1 nM–300 nM) were established. The response of each agonist dose was normalized to the effect of 100 mM K^+. In a third series of experiments, relaxation to ACh (1 nM–10 μM) or DEA/NO (1 nM–10 μM) was measured in precontracted aortic rings in the absence and presence of PVAT using the protocol described above.

3.3. Langendorff perfusion of isolated hearts

Mice were euthanized by inhalation of CO_2 as recommended by the Austrian law on experimentation with laboratory animals. Hearts were rapidly excised and arrested in ice-cold Krebs–Henseleit buffer. After cannulation of the aorta with a 20 gauge needle, retrograde perfusion was established at a constant flow of 20 ml/min/g wet weight with a modified Krebs–Henseleit bicarbonate buffer, pH 7.4 (118 mM NaCl, 25 mM $NaHCO_3$, 1.2 mM KH_2PO_4, 4.8 mM KCl, 1.2 mM $MgSO_4$, 1.25 mM $CaCl_2$, 11 mM D-glucose) using the ISO-HEART perfusion system (Hugo Sachs Elektronik, March-Hugstetten, Germany) as previously described [10]. The perfusate was filtered through a 5 μm filter before infusion and continuously gassed with carbogen (95% O_2, 5% CO_2). Heart temperature, measured with a physitemp probe (Physitemp Instruments, Clifton, NJ), was maintained at 37 °C throughout the experiment. After removal of the left auricle, a tiny fluid-filled balloon, made of a small square of a polyethylene film, was inserted into the left ventricle and connected to a pressure transducer *via* a 4 F biluminal monitoring catheter (Vygon, Aachen, Germany). The following cardiac parameters were monitored using the PLUGSYS data acquisition and control setup for circulatory studies (Hugo Sachs Elektronik, March-Hugstetten, Germany) and recorded using a PowerLab system (ADInstruments Ldt, Hastings, UK): left-ventricular end-diastolic pressure, peak left-ventricular systolic pressure, left-ventricular developed pressure, maximum rate of rise and fall of left ventricular pressure, heart rate (obtained from the pressure signal using a differentiator and heart rate module, respectively) and, as a measure for coronary vessel function, coronary perfusion pressure (CPP; *via* a second pressure transducer attached to the aortic cannula). After establishing stable perfusion conditions (30 min equilibration), bradykinin (BK; 1 nM–3 μM) was added *via* a sideline to the perfusion medium and changes in CPP recorded.

3.4. Cell culture

The microvascular endothelial cell line (MyEnd) was established from mouse hearts by immortalization with polyoma middle T oncogene as described previously [11]. The retrovirus packing cell line GP + E − 86 [12] was kindly provided by B. Engelhardt (Theodor Kocher Institute, Bern, Switzerland). MyEnd cells were immunopositive for the endothelial markers vascular endothelial cadherin and cluster of differentiation 31 (CD31). Cells were grown in Dulbecco's Modified Eagle Medium (DMEM; Life Technologies, Karlsruhe, Germany) supplemented with 100 U/ml penicillin, 0.1 mg/ml streptomycin, 1.25 μg/ml amphotericin B, and 10% (v/v) heat-inactivated fetal calf serum (PPA Laboratories GmbH, Vienna, Austria) in humidified atmosphere (95% O_2/5% CO_2) at 37 °C. Passages 1–5 were used for experiments. MyEnd cells formed monolayers of highly elongated cells frequently organized into whirl-like formations. The overall cell shape and growth pattern resembled that of primary cultures of microvascular endothelial cells from brain and skin [13,14] and differed significantly from the typical cobblestone pattern formed by macrovascular endothelial cells from various sources [15].

3.5. Incorporation and release of [^{3}H]oleate

MyEnd cells seeded on 12-well plates were incubated for 20 h in DMEM (low glucose), containing 400 μM oleic acid complexed with fatty acid-free bovine serum albumin (BSA) and esterified [^{3}H] oleic acid (~$5 * 10^5$ cpm; Hartmann Analytic GmbH, Braunschweig, Germany) as radiolabeled tracer. After removal of medium, cells were washed with phosphate-buffered saline (PBS). Lipids were extracted with ice-cold hexane/isopropanol (3:2) and the solvent was evaporated under a gentle stream of nitrogen. Lipids were resuspended in chloroform, transferred onto TLC silica gel 60 plates (Merck, Darmstadt, Germany) and separated using hexane/diethylether/acetic acid (70:29:1) as solvent. Plates were stained with iodine and mono-, di-, and triglycerides were identified by comparison with an analytical lipid standard mix (Sigma, Vienna, Austria). Radioactive spots containing triglycerides were excised and radioactivity determined by liquid scintillation counting. Results were expressed as cpm/mg protein. In another series of experiments, release of [^{3}H]oleic acid, which had been incorporated into intracellular triglycerides, was induced by addition of 2% fatty acid-free BSA. After incubation for 4 h, extraction and separation of lipid products and quantification of [^{3}H]oleic acid were performed as described above. To measure incorporation of glucose-derived carbon into the cellular triglyceride pool MyEnd cells were challenged with [^{14}C]glucose (0.1 μCi/ml) in the absence and presence of 400 μM non-labeled oleic acid for 20 h. Extraction, separation, and quantification of triglycerides were performed as described above.

3.6. Real-time and conventional PCR

Total RNA was isolated from cells and homogenized tissues using the GenElute™ Mammalian Total RNA Miniprep Kit (Sigma, Vienna, Austria) including DNAse (Sigma, Vienna, Austria) treatment of samples. RNA was transcribed to cDNA using the High Capacity cDNA Reverse Transcription Kit (Applied Biosystems, Vienna, Austria). Real-time PCR analysis was performed with ~30 ng cDNA using TaqMan® Universal PCR Master Mix and pre-designed TaqMan® Gene Expression Assays for endothelial NO synthase (eNOS; Mm00435204_m1), NADPH oxidase 2 subunit (NOX2; Mm00432775_m1), tumor necrosis factor α (TNFα; Mm00443258_m1), monocyte chemotactic protein-1 (MCP-1; Mm00441243_g1), interleukin 6; (IL-6; Mm00446190_m1), heme oxygenase-1 (HO-1; Mm00516005_m1_F), and SOD-1 (Mm01700393_g1). Reactions were carried out on a 7300 Real-Time PCR System (Applied Biosystems, Vienna, Austria). Cycling conditions were as follows: 2 min at 50 °C, 10 min at 95 °C, 40 cycles of 15 s at 95 °C and for 1 min at 60 °C. Data were analyzed according to the $2^{-\Delta\Delta Ct}$ method using cyclophilin (Mm00835365_g1) as reference gene. Lack of amplification was verified in no-template controls. Splicing of XBP1 mRNA was analyzed by conventional PCR using the following primers TTACGAGAGAAAACTCATGGCC (fwd); GGGTCCAAGTTGTCCAGAATGC (rev) [16]. Amplification products were separated by agarose gel electrophoresis (3%).

3.7. Western blot analysis

Tissues were homogenized in 5–10 volumes of RIPA lysis buffer (Sigma, Vienna, Austria) containing 0.5 mM ethylenediaminetetraacetic acid (EDTA), protease and phosphatase inhibitors (Complete™; PhosSTOP™; Roche, Vienna, Austria) using a glass potter Elvehjem homogenizer. Homogenates prepared from PVAT were centrifuged for 10 min at 1000 *g* (4 °C) and lipid-free infranatants were collected and used for Western blot analysis. Endothelial cells were harvested and homogenized by repeated sonication on ice. Denatured samples (10–30 μg) were separated by SDS-PAGE (8% or 10% gels) and transferred onto nitrocellulose membranes. After blocking with Tris-buffered saline containing 0.1% (v/v) Tween-20 and 5% nonfat dry milk or 5% BSA for 1 h (ambient temperature) membranes were incubated overnight at 4 °C with antibodies against ATGL (1:1000; Cell Signaling through New England Biolabs, Frankfurt, Germany), eNOS (1:2000; BD Transduction Laboratories, Heidelberg, Germany), Ser^{1177}phospho-eNOS (1:1000; BD Transduction Laboratories), vasodilator-stimulated phosphoprotein (VASP; 1:1000; Cell Signaling), Ser^{239}phospho-VASP (1:1000; Calbiochem through VWR, Vienna, Austria), NOX2 (1:5000; BD Transduction Laboratories), p67^{phox} (1:5000; BD Transduction Laboratories), p47^{phox} (1:1000; Novus Biologicals, Cambridge, UK), NOX4 (1:1000; Abcam, Cambridge, UK), SOD-1 (1:1000; Santa Cruz Biotechnology, Inc., Heidelberg, Germany), ubiquitin (1:4000; Dako, Vienna, Austria), proteasome 20S core subunit (1:1000; Enzo Life Sciences AG, Lausen, Switzerland), galectin-3 (Mac-2; 1:10,000; Cedarlane through Szabo-Scandic, Vienna, Austria), α-tubulin (1:10,000; Sigma, Vienna, Austria), binding immunglobulin protein (BIP; 1:1000; Cell Signaling), heat shock protein 90 (Hsp90; 1:1000; Cell Signaling), inositol-requiring enzyme 1α (IRE-1α; 1:1000; Cell Signaling), and glyceraldehyde-3-phosphate dehydrogenase (GAPDH; 1:50,000; Sigma). After incubation of membranes with respective horseradish peroxidase-conjugated anti-rabbit or anti-mouse IgG (1:5000) immunoreactive bands were visualized by chemiluminescence using ChemiGlow™ (Biozym, Vienna, Austria) and quantified densitometrically using the E.A.S.Y. Win 32 software (Herolab, Vienna, Austria). Purified human eNOS expressed in *Pichia pastoris* was used as standard [17].

3.8. Determination of NOS activity

Aortas were homogenized in 0.15 ml of a 50 mM triethanolamine/HCl buffer (pH 7.4) containing 1% (v/v) ß-mercaptoethanol, 10 mM 3-[(3-cholamidopropyl)dimethyl-ammonio]-1-propanesulfonate, 0.5 mM EDTA and Complete™ using a glass potter Elvehjem homogenizer. Homogenates were centrifuged at 10,000 *g* for 10 min at 4 °C. Supernatants were assayed for NOS activity as conversion of [^{3}H]L-arginine (~10^5 cpm; Perkin Elmer, Vienna, Austria) to [^{3}H]L-citrulline as previously described [18]. Results were corrected for enzyme-deficient blanks and recovery of L-citrulline. NOS activity of intact MyEnd cells was determined as previously described [19]. Cells were incubated for 10 min at 37 °C in 1 ml of 50 mM Tris–HCl (pH 7.4) containing 100 mM NaCl, 5 mM KCl, 3 mM $CaCl_2$, and 1 mM $MgCl_2$ with [^{3}H] L-arginine (~10^6 cpm) in the absence and presence of ACh (10 μM) or ionomycin (1 μM). Thereafter, cells were washed with 1 ml chilled nominally Ca^{2+}-free incubation buffer and lysed in 10 mM HCl for 1 h at per ambient temperature. Aliquots of 0.1 ml were removed for determination of incorporated radioactivity. Samples were adjusted to pH 5.0 with 0.2 M sodium acetate buffer, containing 10 mM L-citrulline (pH 13.0). [^{3}H]L-citrulline was separated from [^{3}H]L-arginine by cation

exchange chromatography, and radioactivity measured by liquid scintillation counting. Cellular NOS activity is expressed as % of [^{3}H]L-citrulline formed from incorporated [^{3}H]L-arginine.

3.9. Determination of NADPH oxidase activity

MyEnd cells seeded on 6-well plates were homogenized in 0.5 ml PBS containing Complete™ by repeated sonication on ice. Homogenates containing 50–100 μg of protein were incubated in PBS, containing diethylenetriamine pentaacetic acid (0.1 mM) at 37 °C for 30 min in the absence or presence of the NADPH oxidase inhibitor gp91ds-*dat* (50 μM) [9]. Subsequently, NADPH (0.3 mM) and lucigenin (5 μM) were added [20] and lucigenin-derived chemiluminescence (CL) was measured every 10 s for 5 min using a TriCarb® 2100TR Liquid Scintillation Counter (Perkin Elmer, Vienna, Austria). Results were corrected for protein-deficient blanks and expressed as cpm/mg protein.

3.10. Tissue triglyceride hydrolase assay

Lipolytic activities of aorta and white adipose tissue (WAT) were determined using the triglyceride hydrolase assay as described recently [21]. Tissues were homogenized in a solution containing 0.25 M sucrose, 1 mM EDTA, 1 mM dithiothreitol, and Complete™ (pH 7.0) using a glass potter Elvehjem homogenizer, and homogenates were centrifuged at 20,000 *g* for 30 min at 4 °C. Infranatants were collected and aliquots (~30 μg) incubated with 0.15 mM [^{3}H]triolein (~10^6 cpm; Perkin Elmer, Vienna, Austria) as radioactive tracer. Samples were incubated in a total volume of 0.2 ml for 1 h at 37 °C and reactions terminated by addition of 3.25 ml methanol/chloroform/heptane (10:9:7) and 1 ml of 0.1 M K_2CO_3/0.1 M H_3BO_3 (pH 10.5). Samples were centrifuged at 800 *g* for 20 min at an ambient temperature and 1 ml aliquots of the upper phase were collected. Radioactivity was determined by liquid scintillation counting.

3.11. Adipose H_2O_2 formation

H_2O_2 release from PVAT was measured using 10-acetyl-3,7-dihydroxyphenoxazine (Ampliflu) according to the manufacturer's protocol of Amplex® Red Hydrogen Peroxide/Peroxidase Assay Kit (Life Technologies, Vienna, Austria). Freshly isolated PVAT from WT and AKO mice was cut into two pieces of 5–15 mg. Tissue was incubated in a mixture of 750 μl Krebs–Ringer buffer (145 mM NaCl, 4.86 mM KCl, 5.70 mM NaH_2PO_4, 0.54 mM $CaCl_2$, 1.22 mM $MgCl_2$, 5.5 mM glucose; pH 7.4) and 150 μl reaction buffer (10 mM Ampliflu and 10 U/ml horseradish peroxidase in Krebs–Ringer buffer) for 1 h at 37 °C in the absence and presence of catalase (250 U/ml). H_2O_2 release into the incubation buffer was quantified by the horseradish peroxidase-catalyzed oxidation of 10-acetyl-3,7-dihydroxy-phenoxazine to the fluorescent product resorufin at excitation and emission maxima of 571 nm and 585 nm, respectively. PVAT was homogenized in Krebs–Ringer buffer using a glass potter Elvehjem homogenizer and protein concentrations were measured with the Thermo Scientific Pierce BCA™ Protein Assay Kit.

3.12. Scanning electron microscopy

Anesthetized mice were pinned in supine position onto a wax plate, the chest was opened by sternotomy, the ascending aorta was exposed and a ligature from thread was placed around its proximal portion. Thereafter, a hole was punched into the apex of the left ventricle and a bluntly grinded veinflow catheter G21 was introduced *via* the hole into the ascending aorta under stereomicroscopic control using a micromanipulator. The cannula was placed slightly distally to the ligature, the latter was closed, the left atrium was incised and rinsing of the circulatory system with 0.9% NaCl solution was started (flow rates: 70–99 ml/h; volume of perfusate: 7.5–10 ml; duration of rinsing: 6–8 min). When clear efflux escaped the left atrium, perfusion with buffered 2.5% glutaraldehyde in 0.1 M sodium cacodylate buffer (pH 7.35) was started *via* the same route (flow rates: 70–99 ml/h; volume perfused: 10 ml; duration of fixation: 4–7 min). Then, thoracic aortas were excised under binocular control and immersed under fresh fixative for 2 h at room temperature. After two washes for 30 min aortas were transferred into 70% ethanol and stored overnight at 4 °C. Then, aortas were cut into three segments which were cut longitudinally into two halves with razor blades while submerged in 70% ethanol. Specimens were dehydrated in a graded series of ethanol (80%, 90%, and 96% for 30 min each; 100I, 100II, and 100III for 20 min each) and critical point dried *via* carbon dioxide. Dry specimens were mounted onto specimen stubs by colloidal silver, evaporated with carbon and gold, sputtered with gold, and examined in the scanning electron microscope XL-30 (FEI, Eindhoven, The Netherlands) at an accelerating voltage of 20 kV. If necessary, brightness and contrast of micrographs taken were adjusted by the Adobe Photoshop 7.0 software.

3.13. Immunohistochemistry and H&E staining

Thoracic aortas were formalin-fixed, paraffin-embedded, and sectioned. Sections were either stained with hematoxylin and eosin (H&E) according to a standard protocol or labeled for immunohistochemistry by incubating with anti-mouse CD31 (1:50; Thermo Scientific, Vienna, Austria) or anti-mouse α-smooth muscle actin (α-SMA; 1:50; Abcam, Cambridge, UK) for 1 h at ambient temperature. Subsequently, specimens were incubated with HRP Polymers (TL-060-HL; Thermo Scientific, Vienna, Austria) or the AEC system (Dako, Vienna, Austria) for visualization of CD31 and α-SMA, respectively. Analysis was performed with a Nikon Eclipse 80i microscope supplied with camera and using the NIS-Elements D software.

3.14. Protein quantification

Protein concentrations were either measured by the method of Bradford [22] or with the Thermo Scientific Pierce BCA™ Protein Assay Kit (Fisher Scientific Austria GmbH, Vienna, Austria) using BSA as standard.

3.15. Statistics

Concentration–response curves established in aortic ring experiments were fitted to a Hill-type model giving estimates of agonist potency (EC_{50}) and efficacy (E_{max}). Concentration–response curves of different ring segments from a single animal were averaged and counted as individual experiment. ANOVA with post hoc Bonferroni–Dunne test was used for comparison between groups using StatView® (Version 5.0). Experiments performed with aortas, WAT and MyEnd cells were, unless otherwise indicated, analyzed using the unpaired Student's *t*-test. Significance was assumed at $P < 0.05$. Data are presented as mean values ± SEM of n experiments.

4. Results

4.1. Endothelium-dependent vessel function is abolished in ATGL deficiency

The vasodilatory potency of the endothelium-dependent agonist ACh was studied with precontracted aortic rings isolated from WT and AKO mice. As shown in Fig. 1A, ACh relaxed WT vessels in a concentration-dependent manner with an EC_{50} of 240 ± 70 nM and a maximal effect of 67 ± 5% relaxation. The effect of ACh was completely inhibited by the NO synthase (NOS) inhibitor N^G-nitro-L-arginine (data not shown). In contrast to WT vessels, AKO aortas responded only marginally to ACh (17 ± 3% relaxation). Chronic treatment of AKO mice with the PPARα agonist Wy14,643 (which restores cardiac contractility [2]) led to a ~50% improved ACh response (42 ± 2% maximal

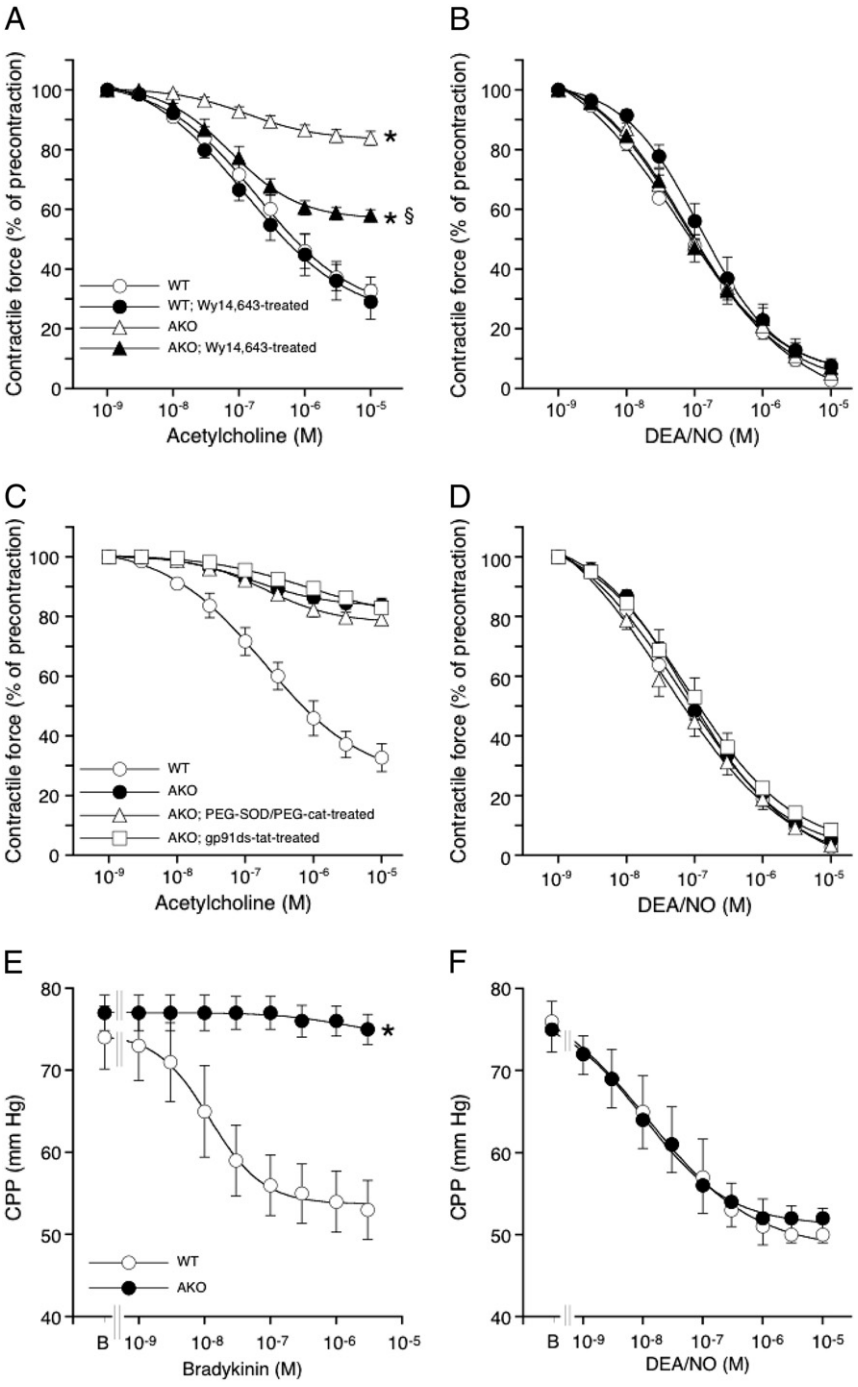

Fig. 1. ATGL deficiency causes severe endothelial dysfunction. (A) Aortic relaxation to ACh was impaired in AKO mice. The relaxant response was partially restored by treatment with the PPARα agonist Wy14,643. Vasorelaxation to DEA/NO was not affected. (C) Treatment with the NADPH oxidase inhibitor gp91ds-*dat* (50 μM) or a combination of PEG-SOD (100 U/ml) and PEG-cat (500 U/ml) did not restore the relaxant response to ACh. (D) Neither gp91ds-*dat* nor PEG-SOD/PEG-cat affected relaxation to DEA/NO. (E) Relaxation of coronary arteries to BK was severely impaired in ATGL-deficient hearts. (F) The dilatory response of coronary vessels to DEA/NO was not affected. Results represent mean values ± SEM of 5 individual experiments. *P < 0.05 *vs* WT; §P < 0.05 *vs* AKO.

relaxation). None of the interventions significantly affected the potency of ACh. As indicated by a preserved response of the rings to the NO donor DEA/NO (Fig. 1B) and adequate contraction to K^+ and to a thromboxane receptor agonist (see Fig. 5 below), impaired relaxation to ACh did not involve dysfunction of vascular smooth muscle cells. Preincubation of aortic rings with either a combination of cell-permeable PEG-SOD and PEG-cat or the selective peptide inhibitor of NADPH oxidases, gp91ds-*dat*, failed to restore the effect of ACh in ATGL deficiency (Fig. 1C). These agents neither affected relaxation to DEA/NO (Fig. 1D), excluding a significant role of superoxide-mediated inactivation of endothelium-derived NO in this experimental setup. The function of microvascular endothelial cells was tested by measuring CPP of isolated hearts in response to the endothelium-dependent vasodilator BK. While the compound decreased CPP in WT hearts in a concentration-dependent manner (EC_{50} = 12 ± 1 nM), the agonist was ineffective in AKO hearts (Fig. 1E). As observed with aortic rings, ATGL deficiency did not affect microvascular relaxation to the NO donor DEA/NO (Fig. 1F).

4.2. Aortic eNOS/cGMP signaling is downregulated in ATGL deficiency

ATGL has been identified and characterized in a variety of tissues and cell types (for review, see [23]), but there is sparse knowledge about ATGL expression in blood vessels. As shown in Fig. 2A, functionally active ATGL was detected in aortic homogenates of WT mice. Protein expression levels and triglyceride hydrolase activity were ~25% and ~5%, respectively, of the values measured in WAT of WT mice. Various biochemical parameters of NO signaling were measured in aortas from WT and genetically modified mice. Protein expression of eNOS was decreased to less than 40% in AKO aortas (Fig. 2B). ATGL deficiency had similar effects on the levels of eNOS phosphorylation at Ser^{1177} (Fig. 2B) and enzyme activity measured as L-arginine to L-citrulline conversion (Fig. 2C). Representative Western blots are shown in Fig. 2H. Treatment of AKO mice with the PPARα agonist Wy14,643 completely restored NOS activity in vascular preparations (Fig. 2C) indicating that the observed effect on eNOS is due to cardiac dysfunction. Aortic eNOS mRNA levels were only marginally affected. Albeit there was a tendency towards increased levels in ATGL deficiency, results did not reach statistical significance (Fig. 2D). Phosphorylation of cytoskeleton-associated VASP at Ser^{239}, which represents a reliable biochemical marker for the function of the NO/cGMP pathway [24], was abolished in AKO aortas (Fig. 2E, H). Surprisingly, expression of VASP protein was also significantly reduced in ATGL-deficient vessels (Fig. 2E, H). Decreased eNOS protein expression despite of unchanged mRNA levels suggested that protein stability was affected in ATGL-deficient vessels. Therefore, we tested for activation of the proteasome by measuring levels of ubiquitinated proteins in aortic homogenates [25]. As shown in Fig. 2F, the total amount of ubiquitinated proteins was significantly reduced in ATGL-deficient aortas. Additionally, aortic protein expression of the 20S core protein (which comprises the protease-like catalytic sites of the 26S proteasome) was increased more than 4-fold in ATGL deficiency (Fig. 2G, H), corroborating the hypothesis of enhanced proteasomal degradation. Aortic mRNA levels of the inflammation marker TNFα were increased nearly 4-fold in ATGL deficiency (Fig. 2I).

To test if vascular ER stress is involved in activation of the proteasome we measured key determinants of the UPR (Fig. S1). The IRE-1/XBP1 branch of the vascular UPR was not significantly affected in ATGL deficiency. Similarly, protein levels of ER-resident chaperons BIP, PDI, Hsp90 were not significantly altered in aortas of AKO mice.

4.3. Characterization of ATGL-deficient endothelial cells

To investigate the endothelial defect on a cellular level, a model of microvascular ATGL-deficient endothelial cells was created from AKO hearts (Fig. 3A) and characterized in terms of NO signaling and related signaling pathways. Cellular ATGL deficiency was confirmed as lack of mRNA (data not shown) and protein expression (see Fig. 3J for a representative Western blot). In ATGL-deficient endothelial cells ~12-fold higher incorporation of [^{3}H]oleate into triglycerides was observed as compared to WT cells (Fig. 3B). Moreover, lipolytic breakdown of [^{3}H]oleate-containing triglycerides was not detected in ATGL-deficient cells, whereas more than 60% of [^{3}H]oleate-containing triglycerides were catabolized in WT cells (Fig. 3B). Challenging of cells with [^{14}C]glucose resulted in significantly increased incorporation of glucose-derived carbon matrix into the cellular triglyceride pool under both basal (Fig. 3C) and oleate-loaded (data not shown) conditions. In marked contrast to the effects observed in isolated aortas, expression

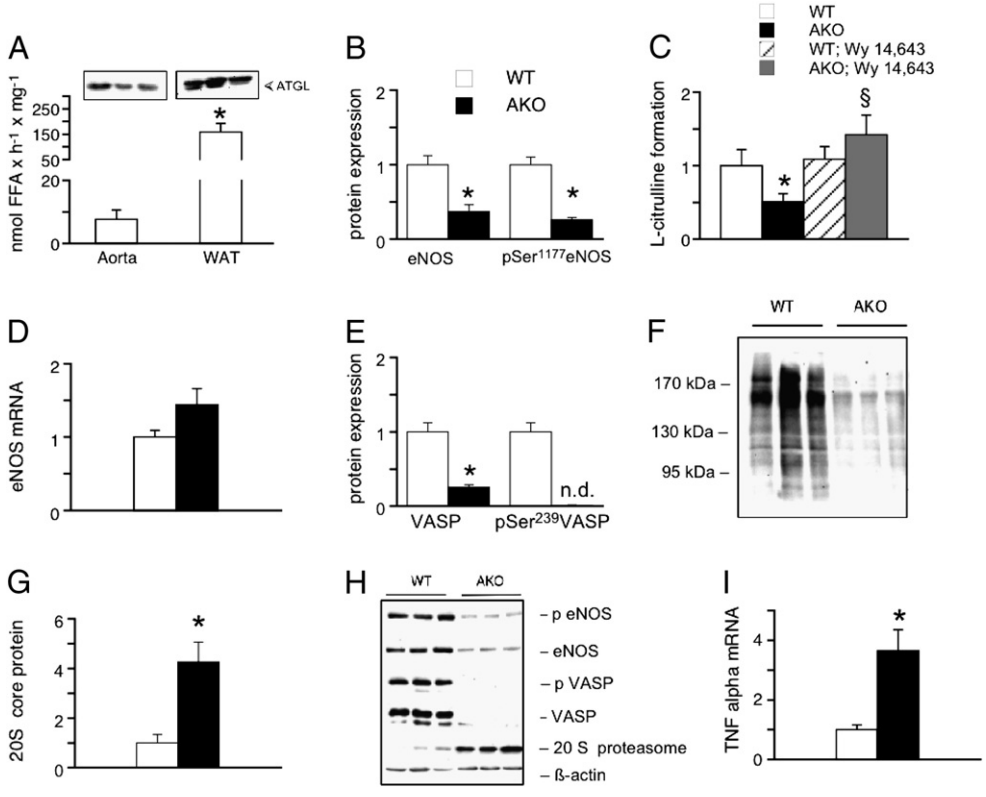

Fig. 2. NO/cGMP signaling is blunted in AKO aortas. (A) ATGL is functionally expressed in WT aortas. Triglyceride hydrolase activity of aortas was compared to that of WAT; n = 4–5; *P < 0.05; aorta *vs* WAT. (B) Protein expression and Ser^{1177} phosphorylation of eNOS were significantly decreased in AKO aortas; *P < 0.05 *vs* WT; n = 12–14. (C) Vascular NOS activity (measured as formation of L-citrulline) was comparably reduced in ATGL deficiency. The effect on enzyme activity was completely reversed in aortas of AKO mice treated with the PPARα agonist Wy14,643. *P < 0.05 *vs* WT; §P < 0.05 AKO (untreated) *vs* AKO (Wy 14,643-treated); n = 4–9. (D) Aortic eNOS mRNA levels; n = 5–8. (E) Protein expression and phosphorylation of VASP at Ser^{239} were decreased in AKO aortas; *P < 0.05 *vs* WT; n = 12–14. (F) Aortic expression of ubiquitinated proteins was markedly decreased in ATGL deficiency. (G) Proteasomal 20S core protein expression was significantly increased in aortas of AKO mice; *P < 0.05 *vs* WT; n = 9. (I) Expression of TNFα mRNA was upregulated in ATGL deficiency; *P < 0.05 *vs* WT; n = 4–5. Except in Fig. A, results are expressed relative to WT controls (=1). Data illustrated in Fig. C were analyzed for statistical significance by ANOVA using Student–Newman–Keuls as post hoc test. Data represent mean values ± SEM of n experiments.

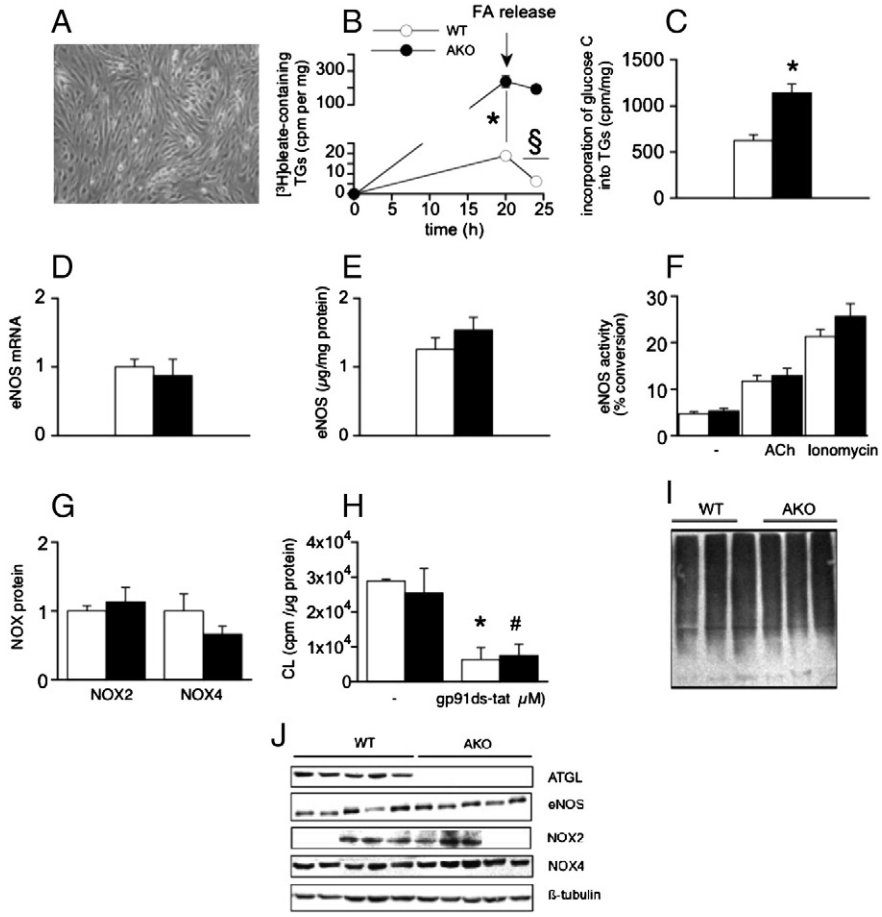

Fig. 3. Generation of microvascular ATGL-deficient endothelial cells. (A, B) Endothelial cells isolated from AKO hearts showed increased capacity of triglyceride storage, impaired lipolytic activity, and (C) increased incorporation of glucose-derived carbon into cellular triglycerides. *P < 0.05; AKO *vs* WT at 20 h; §P < 0.05; WT 20 h *vs* 24 h; n = 3. (D) mRNA (n = 5–6) and (E) protein expression of eNOS (n = 6) as well as (F) basal and stimulated enzyme activity (n = 6–11) were not affected in ATGL-deficient cells. (G) Protein expression of NOX 2 (n = 3) and NOX4 (n = 6) as well as (H) NADPH oxidase-dependent lucigenin CL (n = 3–4) was similar in WT and AKO cells; *P < 0.05; untreated *vs* gp91ds-*dat*-treated WT; #P < 0.05; untreated *vs* gp91ds-*dat*-treated AKO. (I) Expression of ubiquitinated proteins was not affected by endothelial ATGL deficiency; n = 5. Expression of NOX2 and NOX4 protein as well as eNOS mRNA is presented relative to WT controls (=1). eNOS protein is expressed as µg eNOS per mg total protein using purified eNOS as standard. eNOS activity is expressed as % of [^{3}H]L-citrulline formed from incorporated [^{3}H]L-arginine. Data represent mean values ± SEM of n experiments.

of eNOS mRNA (Fig. 3D) and protein (Fig. 3E) as well as basal and stimulated enzyme activity (Fig. 3F) were not affected by ATGL deficiency. To test whether NO availability is compromised in those cells due to increased formation of reactive oxygen species, cellular superoxide production was measured as lucigenin chemiluminescence and expression levels of the most abundant endothelial NADPH oxidase isoforms. Neither protein expression of NOX2 and NOX4 (Fig. 3G) nor superoxide production (Fig. 3H) was affected. Finally, ubiquitinated protein levels were identical in WT and ATGL-deficient endothelial cells (Fig. 3I). These results clearly indicate that at the level of isolated AKO endothelial cells the major characteristics of endothelial dysfunction are no longer evident.

4.4. Characterization of PVAT

There is increasing evidence suggesting that PVAT modulates blood vessel function by production and release of various vasoactive substances (for reviews, see [26,27]). Therefore, we characterized PVAT associated with thoracic aortas of WT and AKO mice and analyzed for mRNA and protein expression of different inflammatory and oxidative markers. PVAT wet weight was increased nearly 7-fold in AKO mice (Fig. 4A, B). Adipose mRNA levels of the inflammation markers TNFα (Fig. 4C), IL-6 (Fig. 4D), and MCP-1 (Fig. 4E) were raised 3.3 ± 1.0, 4.8 ± 1.0, and 7.9 ± 4.3-fold in ATGL deficiency, respectively. NOX2 was upregulated at both mRNA and protein level (Fig. 4F). Additionally, protein expression of cytosolic NADPH oxidase subunits $p67^{phox}$ and $p47^{phox}$ (Fig. 4G) which initiate NOX2 activation, was significantly increased. Expression of Mac-2 protein was potently upregulated in PVAT of AKO mice (Fig. 4H), indicating massive infiltration of macrophages into PVAT. SOD-1 was significantly reduced at both mRNA (data not shown) and protein level (Fig. 4I) and H_2O_2 release from PVAT showed a tendency to increase in ATGL deficiency, but results did not reach statistical significance (Fig. 4J). mRNA expression of the stress response marker HO-1 was increased 5.6 ± 1.2-fold in PVAT of AKO mice (Fig. 4K). Similar to the results obtained with isolated aortas, protein expression and phosphorylation of eNOS were significantly reduced in PVAT of AKO mice (Fig. 4L). Representative Western blots are shown in Fig. 4M and N. To test if the observed phenotype is related to cardiac dysfunction, PVAT of Wy 14,643-fed WT and AKO mice was analyzed for selected parameters of oxidative and inflammatory stress. Treatment of animals with the PPARα agonist failed to reverse Mac-2, SOD-1, and p67phox protein expression (Fig. S2), suggesting that heart-independent pathological processes are operative in PVAT of AKO mice.

To judge potential functional consequences of PVAT-derived inflammatory oxidative stress we measured contractile and relaxant responses of aortas isolated from WT and AKO mice in the absence and presence of PVAT. As shown in Fig. 5A, vascular contractility to K^+ was similar for all experimental groups. Fig. 5B illustrates the contractile responses of WT and AKO aortas to the thromboxane mimetic U46619.

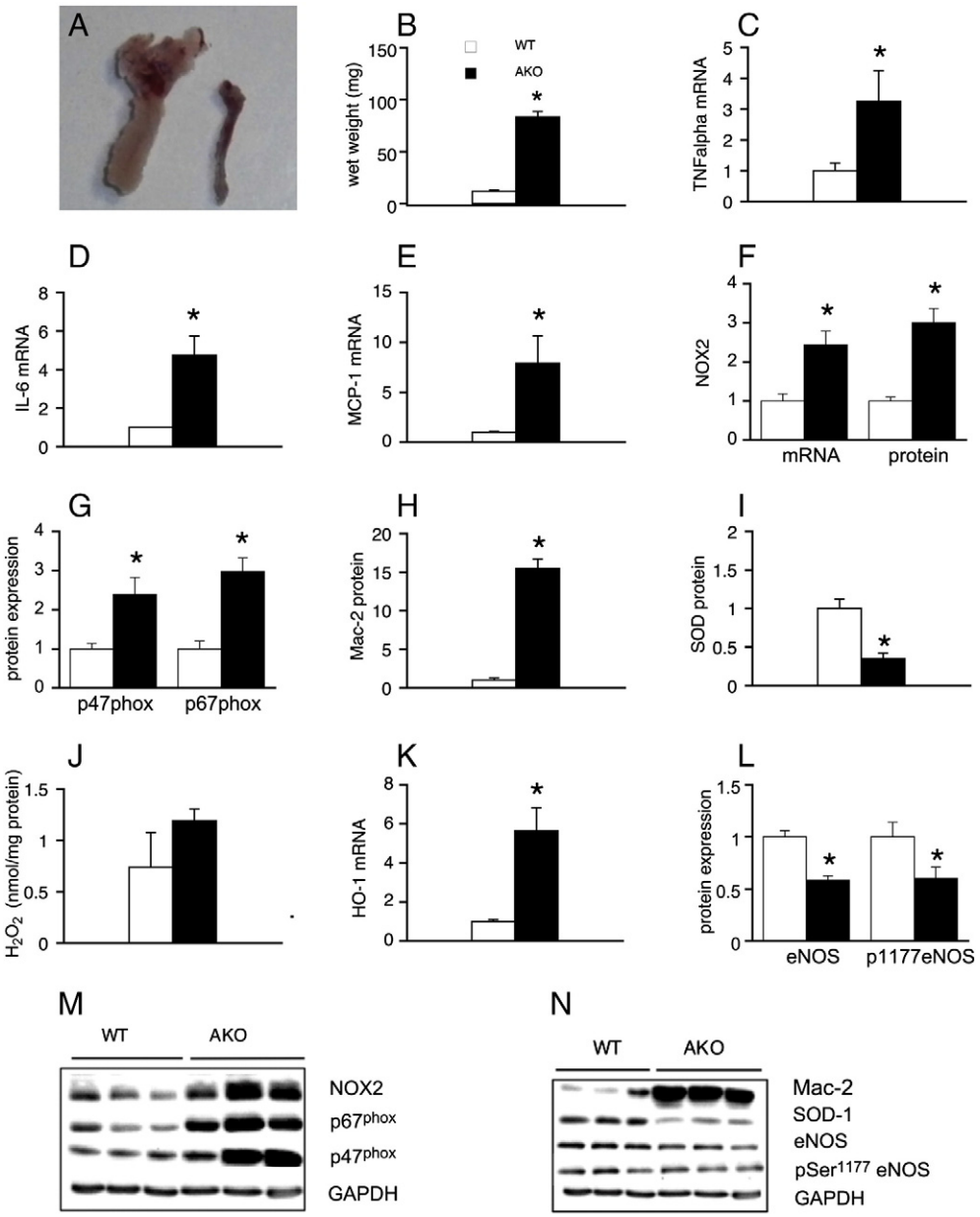

Fig. 4. Characterization of ATGL-deficient PVAT. (A, B) The amount of PVAT surrounding thoracic aortas was substantially increased in AKO mice; *P < 0.05 *vs* WT; n = 30–32. Adipose mRNA expression of (C) TNFα (n = 15), (D) IL-6 (n = 10–11), and (E) MCP-1 (n = 15) was increased in ATGL-deficient PVAT; *P < 0.05 *vs* WT. (F) mRNA and protein expression of NOX2 was upregulated in PVAT of AKO mice; *P < 0.05 *vs* WT; n = 16–18. (G) Protein expression of NOX2-related $p47^{phox}$ (n = 16–17) and $p67^{phox}$ (n = 9–10) subunits was increased; *P < 0.05 *vs* WT. (H) Protein expression of Mac-2 was highly upregulated; *P < 0.05 *vs* WT; n = 6–9. (I) SOD-1 protein was downregulated in PVAT of AKO mice; *P < 0.05 *vs* WT; n = 9. (J) Catalase-inhibited H_2O_2 release from PVAT; n = 7. (K) Adipose mRNA levels of HO-1 were upregulated in ATGL deficiency; *P < 0.05 *vs* WT; n = 7–9. (L) Protein expression and phosphorylation of eNOS were downregulated in PVAT of AKO mice; *P < 0.05 *vs* WT; n = 6–17. Protein and mRNA expression is presented relative to WT controls (=1). Data represent mean values ± SEM of n experiments.

In PVAT-denuded vessels, contractility was identical for both experimental groups. Presence of PVAT, however, significantly reduced the contractile efficacy of U46619 in WT aortas (from 155.1 ± 5.7% to 125.6 ± 9.4%). An even more pronounced effect of PVAT was observed in AKO aortas, with PVAT reducing maximal contractility from 162.9 ± 5.5% to 90.4 ± 9.6%. In contrast to its effects on vascular contractility, PVAT did not affect relaxation to ACh or DEA/NO under any experimental condition (Fig. 5C, D).

4.5. Studies on vessel layer morphology and endothelial integrity

Histological analysis of aortic sections obtained from WT and AKO mice that were stained with H&E showed no microscopic changes in vessel structure or layer morphology (Fig. 6). Labeling of aortic specimens for the endothelial and smooth muscle cell markers CD31 and α-SMA, respectively, revealed similar staining distribution and intensity, excluding prominent histological differences of endothelial and smooth muscle cell layers (Fig. 6). To test for integrity of the vascular endothelium, the luminal morphology of aortas was studied by scanning electron microscopy. In Fig. 7, aortic endothelia of WT (A) and AKO (B) mice are shown in smaller (left panel) and larger (right panel) magnification. Layers of both experimental groups exhibited slightly undulating longitudinal endothelial folds. Endothelial cells of WT aortas showed rhomboid to slender longish shapes with a length of 45–60 μm and a width of 7–12 μm (Fig. 7A, right panel). Cell borders were rather straight with no prominent overlapping of neighboring cells. The endothelial luminal surface of AKO aortas is illustrated in Fig. 7B. Most of endothelial cells were rather stout with a length of 25 μm and a width of

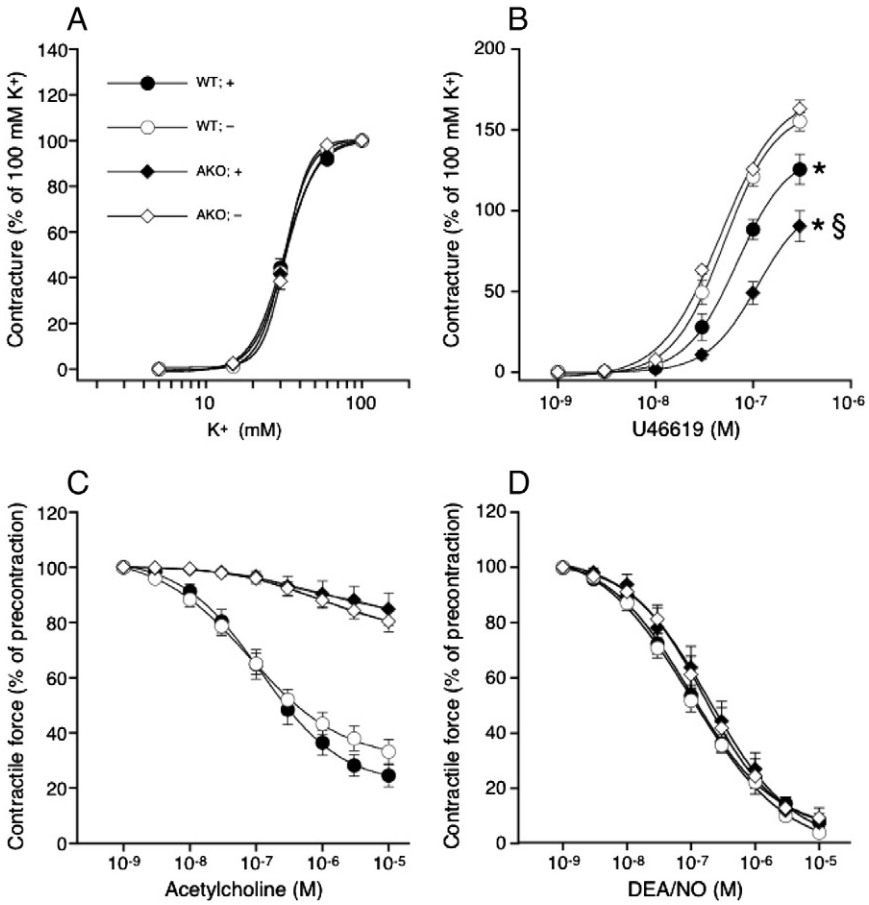

Fig. 5. Effect of PVAT on vessel function. (A) Aortas isolated from WT and AKO mice exhibited comparable contractility to K^+ in the absence and presence of PVAT; n = 4–5. (B) Presence of PVAT reduced the contractile efficacy of U46619 in aortas of AKO mice to a greater extent than in WT mice; *P < 0.05 *vs* PVAT-denuded WT; §P < 0.05 *vs* PVAT-containing WT; n = 4–5. Relaxation to (C) ACh and (D) DEA/NO was not affected by PVAT; n = 4–5. Data represent mean values ± SEM of n individual experiments.

15 μm, but locally also spindle-shaped cells of 60 μm length were observed. Endothelia of both experimental groups revealed endothelial fenestrae with variations in number and size. Based on these results, we have no experimental evidence for disturbances in the microstructural integrity of the endothelial cell barrier.

5. Discussion

This study demonstrates that AKO mice, a rodent model of NLSDM, suffer from severe micro- and macrovascular endothelial dysfunction. Loss of vascular reactivity was partially rescued in AKO mice chronically treated with a PPARα agonist, that restored cardiac function of these animals [2] without exerting direct vasoprotective effects. This suggests that at least two mechanism (one of which is apparently heart-dependent) are operative in endothelial dysfunction.

One component comprises downregulation of eNOS expression in blood vessels. The close relationship between cardiac and vascular dysfunction is well-documented in experimental animals and human surveys (for review, see [4]) and might therefore also exist in AKO mice. Moreover, experimentally-provoked chronic heart failure was reported to result in endothelial dysfunction due to downregulation of vascular eNOS transcription [28]. However, in AKO mice, eNOS mRNA levels were not decreased but rather tended to slightly increase which excludes a transcriptional effect. It has been reported that TNFα causes a substantial decrease in eNOS mRNA stability [29], and TNFα mRNA expression is indeed increased in several tissues of AKO mice (this study [30]). Since plasma TNFα levels were beyond the detection limit of the assay in both experimental groups (data not shown), we cannot judge the contribution of circulating TNFα to vascular eNOS downregulation. However, our data point to an alternative explanation involving proteasomal degradation of eNOS protein in AKO vessels. It has been reported recently that selective inhibition of the 26S proteasome caused upregulation of eNOS in cultured endothelial cells and improved endothelial function of isolated aortas [25]. This finding agrees well with our observations showing the inverse effect *i.e.* decreased eNOS protein expression in AKO vessels accompanied by a significant loss of ubiquitinated proteins indicating enhanced proteasomal activity. Moreover, the proteasomal 20S core subunit (which comprises the protease-like catalytic sites of the 26S proteasome machinery) was significantly upregulated in vessels of AKO mice.

So far, we have been unable to identify the mediator(s) that trigger(s) upregulation/activation of the proteasome in ATGL-deficient blood vessels. An obvious culprit that should be considered is oxidative stress. It has been proposed that mild oxidative challenge leads to activation of the 26S proteasome by as yet unknown mechanisms (for review, see [31]). In contrast, prolonged exposure of cells to severe oxidative stress is thought to induce *de novo* biosynthesis of proteasomal proteins and their assembly to functional degradating units in order to cope with accumulating misfolded proteins (for review, see [31]). Our observation that AKO mice suffer from pronounced NADPH oxidase-driven oxidative stress in the heart supports this hypothesis [30]. Moreover, the fact, that the 20S core protein was significantly upregulated in AKO aortas, strengthens this concept. However, endothelial function was not improved upon preincubation of ATGL-deficient rings with either SOD/cat or the NADPH oxidase-specific inhibitor gp91ds-*dat*, questioning a significant contribution of NADPH oxidase-derived

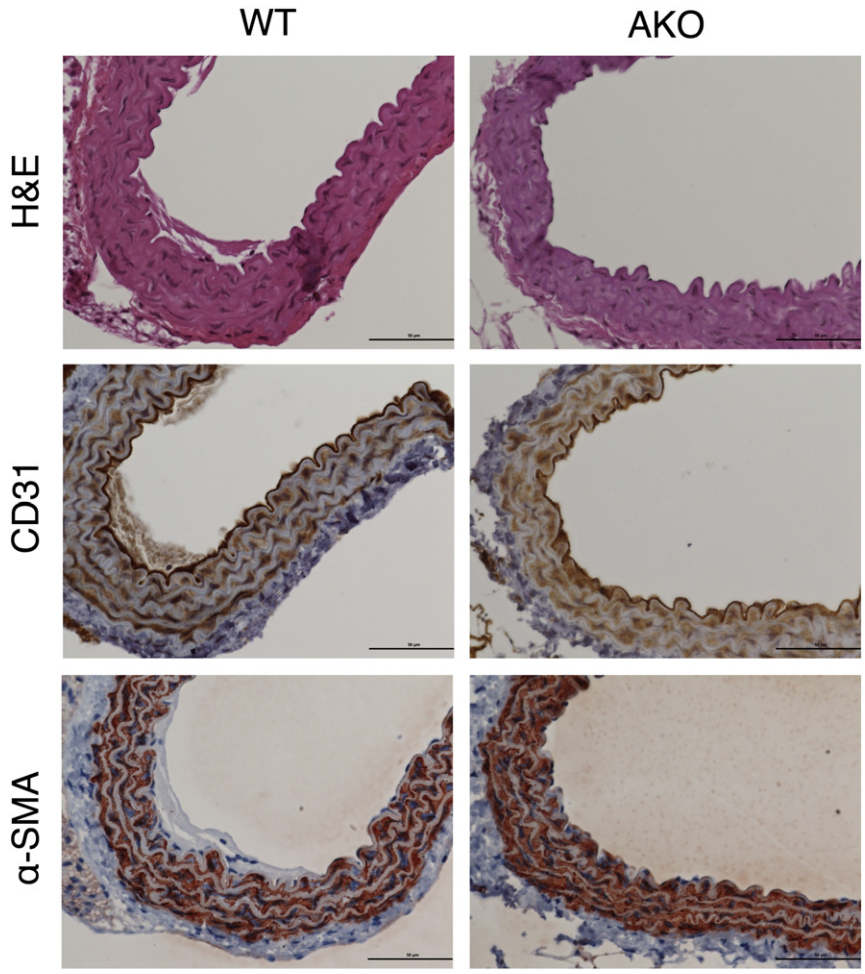

Fig. 6. Histological characterization of WT and AKO aortas. Representative images of WT and AKO specimens stained with H&E showed no morphological changes through all sections of the aorta (upper panels). Endothelial cells labeled with CD31 (middle panel) or smooth muscle cells labeled with α-SMA (lower panel) exhibit similar staining intensity and distribution in sections of WT and AKO aortas. Images are representative for 3 individual experiments.

superoxide. Nonetheless, chronic exposure of the vasculature to oxidative stress may cause irreversible damage of the endothelium, precluding effects of short-term interventions.

To investigate if endothelial dysfunction originates from disturbed endothelial cell homeostasis we studied the effects of ATGL deficiency on NO signaling in a microvascular endothelial cell model. Cells obtained from WT mice expressed small amounts of functionally active ATGL, but the biochemical parameters of NO signaling were identical in ATGL-deficient cells. In particular, the eNOS expression level was not affected by ATGL deficiency, indicating that proteasomal activation in the vasculature is not caused by an intrinsic endothelial process. To test for a potential role of circulating factors that might be missing in the cell culture model, we challenged WT endothelial cells for 48 h with plasma from AKO mice but did not observe any effect on eNOS activity (Mussbacher M; unpublished observation).

Phosphorylation of the protein kinase G target VASP was virtually abolished in ATGL-deficient blood vessels. This finding agrees well with the relaxation data and impressively demonstrates impaired NO signaling in this pathology. Surprisingly, however, the VASP protein was also significantly downregulated in AKO aortas. VASP plays a crucial role in the regulation of actin filament dynamics and is regulated by differential phosphorylation [32]. Endothelial VASP deficiency was found to result in compromised integrin- and cadherin-mediated cytoskeletal anchorage [33]. Therefore, we reasoned that reduced VASP expression in ATGL-deficient aortas might result in compromised integrity of the endothelial cell layer. However, scanning electron microscopic experiments revealed comparable integrity of aortic *endothelia*. Thus, loss of aortic VASP protein appears to be a consequence rather than a cause of endothelial dysfunction and may reflect enhanced proteasomal activity of ATGL-deficient aortas.

PVAT represents another potential source of pathogenic mediators that provoke endothelial dysfunction. Inflammation and oxidative stress in PVAT have recently been linked to endothelial dysfunction in obese experimental animals and adipose humans [34–36]. In particular, it has been suggested that oxidative and inflammatory mediators blunt the anti-contractile effect of PVAT that is generally regarded as beneficial physiological contribution to vascular tone [34]. In AKO mice, aortic PVAT mass was drastically increased. Moreover, we observed pronounced upregulation of NADPH oxidases and several inflammatory markers. Upregulation of HO-1 mRNA expression together with reduced SOD-1 mRNA and protein abundance are further indicators of a pro-oxidative scenario in PVAT of AKO mice. Upregulation of Mac-2 protein, a lectin that is expressed and secreted by macrophages and monocytes [37] and that induces chemotactic, phagocytic, and lipid scavenging processes [38–40] points to severe chronic adipose tissue inflammation. The fact that Wy 14,643 treatment failed to protect AKO mice from PVAT inflammation suggests that heart-independent pathological processes are operative in PVAT of AKO mice.

In functional studies, contraction of WT and AKO aortas to the thromboxane mimetic U46619 was identical in the absence of PVAT. However, PVAT-coated vessels of AKO mice surprisingly showed a significantly attenuated response as compared to WT. In previous studies,

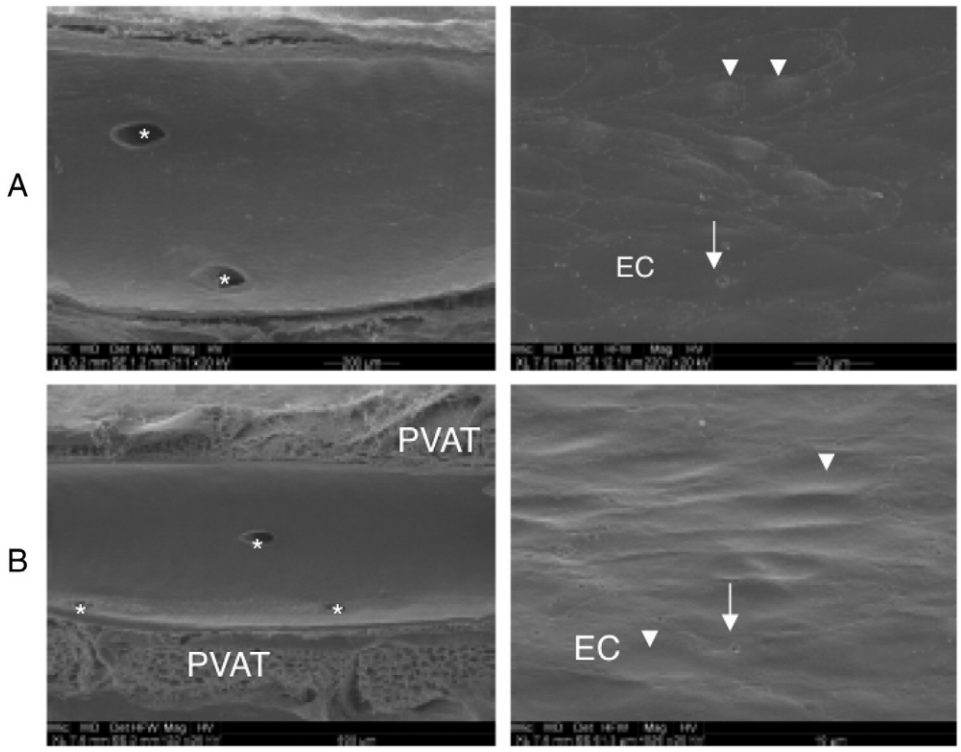

Fig. 7. Scanning electron microscopy of the luminal endothelial surface morphology. Experiments confirm the endothelial integrity of thoracic aorta in WT (A) and AKO (B) mice. Arrows point to round endothelial fenestrae, arrowheads to protruding endothelial cell nuclei. Asterisks mark orifices of abutting intercostal arteries. EC; endothelial cell; horizontal field width: (A) 1.20 mm (left), 110 μm (right); (B) 1.95 mm (left), 60 μm (right). Images are representative for 3 individual experiments.

decreased vascular contractility in the presence of PVAT has been interpreted as beneficial effect and efforts have been made to identify the adipose tissue-derived relaxing factor [41–43]. Our results differ from those of a recent study showing that attenuated contractility in the presence of PVAT is abolished in a mouse model of human metabolic syndrome [36]. The apparent discrepancy may arise from a quite different metabolic profile of the experimental animals used. While AKO mice show increased insulin sensitivity, improved glucose uptake and utilization, and physiological serum triglycerides [1], classical animal models of obesity are characterized by hyperglycemia, hyperinsulinemia, and increased serum triglycerides [35,36]. It is therefore conceivable, that significant differences in perivascular adipocyte and/or vascular smooth muscle cell metabolism lead to opposite functional effects of PVAT.

In summary, we demonstrate that global ATGL deficiency leads to pronounced vascular endothelial dysfunction which is partially due to down-regulation of vascular eNOS expression, presumably *via* upregulation/activation of the 26S proteasome. Moreover, we have demonstrated local PVAT inflammation in AKO mice. More work is needed to clarify the molecular mechanisms behind these unexpected findings and to further characterize the local vascular inflammatory processes that might compromise endothelial function. Our results reveal a hitherto unrecognized link between disturbed lipid metabolism, obesity and cardiovascular disease.

Murine ATGL deficiency is regarded as rodent pendant of NLSDM in humans. This rare genetic disorder is characterized by excessive lipid accumulation in multiple tissues and becomes clinically evident most notably as severe dilated cardiomyopathy. To our current knowledge, vascular function of these patients has not been studied, yet. On the basis of the results we obtained with AKO mice it seems obvious that characterization of vessel function of diseased humans should be included into clinical studies.

Supplementary data to this article can be found online at http://dx.doi.org/10.1016/j.bbalip.2014.03.005.

Acknowledgements

We thank Nikola Golenhofen (Institute of Anatomy and Cell Biology, University of Ulm, Germany) for kindly providing the retrovirus packing cell line GP + E − 86. We thank Silvia Schauer (Institute of Pathology, Medical University of Graz; Austria) and Ines Neubacher (Department of Pharmacology and Toxicology, University of Graz, Austria) for their excellent technical assistance. This work was supported by the Austrian Science Fund (Grants F3003, P24005, W901 DK Molecular Enzymology to B.M, and W1226 DK Metabolic and Cardiovascular Disease to G.H.).

References

[1] G. Haemmerle, A. Lass, R. Zimmermann, G. Gorkiewicz, C. Meyer, J. Rozman, G. Heldmaier, R. Maier, C. Theussl, S. Eder, D. Kratky, E.F. Wagner, M. Klingenspor, G. Hoefler, R. Zechner, Defective lipolysis and altered energy metabolism in mice lacking adipose triglyceride lipase, Science 312 (2006) 734–737.
[2] G. Wölkart, A. Schrammel, K. Dorffel, G. Haemmerle, R. Zechner, B. Mayer, Cardiac dysfunction in adipose triglyceride lipase deficiency: treatment with a PPARalpha agonist, Br. J. Pharmacol. 165 (2012) 380–389.
[3] G. Haemmerle, T. Moustafa, G. Woelkart, S. Buttner, A. Schmidt, T. van de Weijer, M. Hesselink, D. Jaeger, P.C. Kienesberger, K. Zierler, R. Schreiber, T. Eichmann, D. Kolb, P. Kotzbeck, M. Schweiger, M. Kumari, S. Eder, G. Schoiswohl, N. Wongsiriroj, N.M. Pollak, F.P. Radner, K. Preiss-Landl, T. Kolbe, T. Rulicke, B. Pieske, M. Trauner, A. Lass, R. Zimmermann, G. Hoefler, S. Cinti, E.E. Kershaw, P. Schrauwen, F. Madeo, B. Mayer, R. Zechner, ATGL-mediated fat catabolism regulates cardiac mitochondrial function *via* PPAR-alpha and PGC-1, Nat. Med. 17 (2011) 1076–1085.
[4] J. Bauersachs, J.D. Widder, Endothelial dysfunction in heart failure, Pharmacol. Rep. 60 (2008) 119–126.
[5] D. Fischer, S. Rossa, U. Landmesser, S. Spiekermann, N. Engberding, B. Hornig, H. Drexler, Endothelial dysfunction in patients with chronic heart failure is independently associated with increased incidence of hospitalization, cardiac transplantation, or death, Eur. Heart J. 26 (2005) 65–69.
[6] S.D. Katz, K. Hryniewicz, I. Hriljac, K. Balidemaj, C. Dimayuga, A. Hudaihed, A. Yasskiy, Vascular endothelial dysfunction and mortality risk in patients with chronic heart failure, Circulation 111 (2005) 310–314.
[7] K. Hirano, Y. Ikeda, N. Zaima, Y. Sakata, G. Matsumiya, Triglyceride deposit cardiomyovasculopathy, N. Engl. J. Med. 359 (2008) 2396–2398.

[8] J. Fischer, C. Lefevre, E. Morava, J.M. Mussini, P. Laforet, A. Negre-Salvayre, M. Lathrop, R. Salvayre, The gene encoding adipose triglyceride lipase (PNPLA2) is mutated in neutral lipid storage disease with myopathy, Nat. Genet. 39 (2007) 28–30.
[9] M.E. Cifuentes, F.E. Rey, O.A. Carretero, P.J. Pagano, Upregulation of p67(phox) and gp91(phox) in aortas from angiotensin II-infused mice, Am. J. Physiol. 279 (2000) H2234–H2240.
[10] F. Brunner, P. Andrew, G. Wölkart, R. Zechner, B. Mayer, Myocardial contractile function and heart rate in mice with myocyte-specific overexpression of endothelial nitric oxide synthase, Circulation 104 (2001) 3097–3102.
[11] N. Golenhofen, W. Ness, E.F. Wawrousek, D. Drenckhahn, Expression and induction of the stress protein alpha-B-crystallin in vascular endothelial cells, Histochem. Cell Biol. 117 (2002) 203–209.
[12] D. Markowitz, S. Goff, A. Bank, A safe packaging line for gene transfer: separating viral genes on two different plasmids, J. Virol. 62 (1988) 1120–1124.
[13] M.A. Karasek, Microvascular endothelial cell culture, J. Invest. Dermatol. 93 (1989) 33S–38S.
[14] L.L. Rubin, K. Barbu, F. Bard, C. Cannon, D.E. Hall, H. Horner, M. Janatpour, C. Liaw, K. Manning, J. Morales, et al., Differentiation of brain endothelial cells in cell culture, Ann. N. Y. Acad. Sci. 633 (1991) 420–425.
[15] H.J. Schnittler, B. Puschel, D. Drenckhahn, Role of cadherins and plakoglobin in interendothelial adhesion under resting conditions and shear stress, Am. J. Physiol. 273 (1997) H2396–H2405.
[16] K. Cawley, S. Deegan, A. Samali, S. Gupta, Assays for detecting the unfolded protein response, Methods Enzymol. 490 (2011) 31–51.
[17] A. Leber, B. Hemmens, B. Klosch, W. Goessler, G. Raber, B. Mayer, K. Schmidt, Characterization of recombinant human endothelial nitric-oxide synthase purified from the yeast *Pichia pastoris*, J. Biol. Chem. 274 (1999) 37658–37664.
[18] B. Mayer, P. Klatt, E.R. Werner, K. Schmidt, Molecular mechanisms of inhibition of porcine brain nitric oxide synthase by the antinociceptive drug 7-nitro-indazole, Neuropharmacology 33 (1994) 1253–1259.
[19] K. Schmidt, B. Mayer, Assay of tissue activity of nitric oxide synthase, in: M. Maines, L. Costa, D.M. Reed, S. Sassa, J.W.S. Inc (Eds.), Curr Protoc Toxicol, 1999, (New York).
[20] Y. Li, H. Zhu, P. Kuppusamy, V. Roubaud, J.L. Zweier, M.A. Trush, Validation of lucigenin (bis-N-methylacridinium) as a chemilumigenic probe for detecting superoxide anion radical production by enzymatic and cellular systems, J. Biol. Chem. 273 (1998) 2015–2023.
[21] M. Schweiger, R. Schreiber, G. Haemmerle, A. Lass, C. Fledelius, P. Jacobsen, H. Tornqvist, R. Zechner, R. Zimmermann, Adipose triglyceride lipase and hormone-sensitive lipase are the major enzymes in adipose tissue triacylglycerol catabolism, J. Biol. Chem. 281 (2006) 40236–40241.
[22] M.M. Bradford, A rapid and sensitive method for the quantitation of microgram quantities of protein utilizing the principle of protein–dye binding, Anal. Biochem. 72 (1976) 248–254.
[23] R. Zechner, P.C. Kienesberger, G. Haemmerle, R. Zimmermann, A. Lass, Adipose triglyceride lipase and the lipolytic catabolism of cellular fat stores, J. Lipid Res. 50 (2009) 3–21.
[24] M. Oelze, H. Mollnau, N. Hoffmann, A. Warnholtz, M. Bodenschatz, A. Smolenski, U. Walter, M. Skatchkov, T. Meinertz, T. Munzel, Vasodilator-stimulated phosphoprotein serine 239 phosphorylation as a sensitive monitor of defective nitric oxide/cGMP signaling and endothelial dysfunction, Circ. Res. 87 (2000) 999–1005.
[25] V. Stangl, M. Lorenz, S. Meiners, A. Ludwig, C. Bartsch, M. Moobed, A. Vietzke, H.T. Kinkel, G. Baumann, K. Stangl, Long-term up-regulation of eNOS and improvement of endothelial function by inhibition of the ubiquitin–proteasome pathway, FASEB J. 18 (2004) 272–279.
[26] K.A. Britton, C.S. Fox, Perivascular adipose tissue and vascular disease, Clin. Lipidol. 6 (2011) 79–91.
[27] M. Gollasch, Vasodilator signals from perivascular adipose tissue, Br. J. Pharmacol. 165 (2012) 633–642.
[28] C.J. Smith, D. Sun, C. Hoegler, B.S. Roth, X. Zhang, G. Zhao, X.B. Xu, Y. Kobari, K. Pritchard, W.C. Sessa, T.H. Hintze, Reduced gene expression of vascular endothelial NO synthase and cyclooxygenase-1 in heart failure, Circ. Res. 78 (1996) 58–64.
[29] G. Yan, B. You, S.P. Chen, J.K. Liao, J. Sun, Tumor necrosis factor-alpha downregulates endothelial nitric oxide synthase mRNA stability *via* translation elongation factor 1-alpha 1, Circ. Res. 103 (2008) 591–597.
[30] A. Schrammel, M. Mussbacher, S. Winkler, G. Haemmerle, H. Stessel, G. Wölkart, R. Zechner, B. Mayer, Cardiac oxidative stress in a mouse model of neutral lipid storage disease, Biochim. Biophys. Acta (2013), http://dx.doi.org/10.1016/j.bbalip.2013.07.004.
[31] C.T. Aiken, R.M. Kaake, X. Wang, L. Huang, Oxidative stress-mediated regulation of proteasome complexes, Mol. Cell. Proteomics 10 (2011) (R110 006924).
[32] P.M. Benz, C. Blume, S. Seifert, S. Wilhelm, J. Waschke, K. Schuh, F. Gertler, T. Munzel, T. Renne, Differential VASP phosphorylation controls remodeling of the actin cytoskeleton, J. Cell Sci. 122 (2009) 3954–3965.
[33] N. Schlegel, J. Waschke, Impaired integrin-mediated adhesion contributes to reduced barrier properties in VASP-deficient microvascular endothelium, J. Cell. Physiol. 220 (2009) 357–366.
[34] A.S. Greenstein, K. Khavandi, S.B. Withers, K. Sonoyama, O. Clancy, M. Jeziorska, I. Laing, A.P. Yates, P.W. Pemberton, R.A. Malik, A.M. Heagerty, Local inflammation and hypoxia abolish the protective anticontractile properties of perivascular fat in obese patients, Circulation 119 (2009) 1661–1670.
[35] J. Ketonen, T. Pilvi, E. Mervaala, Caloric restriction reverses high-fat diet-induced endothelial dysfunction and vascular superoxide production in C57Bl/6 mice, Heart Vessel. 25 (2010) 254–262.
[36] C. Marchesi, T. Ebrahimian, O. Angulo, P. Paradis, E.L. Schiffrin, Endothelial nitric oxide synthase uncoupling and perivascular adipose oxidative stress and inflammation contribute to vascular dysfunction in a rodent model of metabolic syndrome, Hypertension 54 (2009) 1384–1392.
[37] S. Sato, R.C. Hughes, Regulation of secretion and surface expression of Mac-2, a galactoside-binding protein of macrophages, J. Biol. Chem. 269 (1994) 4424–4430.
[38] S. Cinti, G. Mitchell, G. Barbatelli, I. Murano, E. Ceresi, E. Faloia, S. Wang, M. Fortier, A. S. Greenberg, M.S. Obin, Adipocyte death defines macrophage localization and function in adipose tissue of obese mice and humans, J. Lipid Res. 46 (2005) 2347–2355.
[39] H. Sano, D.K. Hsu, J.R. Apgar, L. Yu, B.B. Sharma, I. Kuwabara, S. Izui, F.T. Liu, Critical role of galectin-3 in phagocytosis by macrophages, J. Clin. Invest. 112 (2003) 389–397.
[40] H. Sano, D.K. Hsu, L. Yu, J.R. Apgar, I. Kuwabara, T. Yamanaka, M. Hirashima, F.T. Liu, Human galectin-3 is a novel chemoattractant for monocytes and macrophages, J. Immunol. 165 (2000) 2156–2164.
[41] G. Fesus, G. Dubrovska, K. Gorzelniak, R. Kluge, Y. Huang, F.C. Luft, M. Gollasch, Adiponectin is a novel humoral vasodilator, Cardiovasc. Res. 75 (2007) 719–727.
[42] Y.J. Gao, C. Lu, L.Y. Su, A.M. Sharma, R.M. Lee, Modulation of vascular function by perivascular adipose tissue: the role of endothelium and hydrogen peroxide, Br. J. Pharmacol. 151 (2007) 323–331.
[43] N. Maenhaut, C. Boydens, J. Van de Voorde, Hypoxia enhances the relaxing influence of perivascular adipose tissue in isolated mice aorta, Eur. J. Pharmacol. 641 (2010) 207–212.